Field evolution of the magnetic structures in $Er_2Ti_2O_7$ through the critical point

H. B. Cao, I. Mirebeau,* and A. Gukasov
Centre de Saclay, DSM/IRAMIS/Laboratoire Léon Brillouin, CEA, 91191 Gif-sur-Yvette, France

P. Bonville
Centre de Saclay, DSM/IRAMIS/Service de Physique de l'Etat Condensé, CEA, 91191 Gif-sur-Yvette, France

C. Decorse
Laboratoire de Physico-Chimie de l'Etat Solide, ICMMO, Université Paris-Sud, 91405 Orsay, France
(Received 2 July 2010; revised manuscript received 7 September 2010; published 28 September 2010)

We have measured neutron-diffraction patterns in a single-crystal sample of the pyrochlore compound $Er_2Ti_2O_7$ in the antiferromagnetic phase (T=0.3 K), as a function of the magnetic field, up to 6 T, applied along the [110] direction. We determine all the characteristics of the magnetic structure throughout the critical point at H_c=2 T. As a main result, all Er moments align along the field at H_c and their values reach a minimum. Using a four-sublattice self-consistent calculation, we show that the evolution of the magnetic structure and the value of the critical field are rather well reproduced using the same anisotropic exchange tensor as that accounting for the local paramagnetic susceptibility. In contrast, an isotropic exchange tensor does not yield the correct moment variations through the critical point. The model also accounts semiquantitatively for other experimental data obtained in previous works, such as the field dependence of the heat capacity, energy of the dispersionless inelastic modes and transition temperature.

DOI: 10.1103/PhysRevB.82.104431 PACS number(s): 75.25.−j, 25.40.Dn, 61.05.fg, 05.30.Rt

I. INTRODUCTION

Geometrical magnetic frustration allows one to obtain materials with tunable properties. It yields a large landscape of possible magnetic ground states due to the inability of the system to choose a unique spin configuration which minimizes the energy. Rare-earth pyrochlores $R_2Ti_2O_7$, where the R magnetic moments reside on the summits of corner sharing tetrahedra, are model systems to study such effects. Here, geometrical frustration does not arise from the competition of magnetic interactions, but rather emerges in the context of a highly symmetrical structure, from the subtle interplay of three main energy terms: the single ion crystal field anisotropy, the exchange interaction and the magnetic dipolar coupling. In $R_2Ti_2O_7$, the trigonal symmetry of the crystal field at the R site comes from the oxygen environment. At low temperature, this yields two generic behaviors, Ising-type (Ho, Dy, and Tb) or XY-like (Er and Yb), depending on whether the ⟨111⟩ axes are easy or hard anisotropy axes for the magnetic moments. The final selection of a magnetic state within the ground state manifold is determined by the nature, length scale and sign of the magnetic interaction, by perturbation energy terms, or by "order by disorder" processes.[1,2]

The spin-ice compounds $Ho_2Ti_2O_7$ and $Dy_2Ti_2O_7$, combining a strong Ising anisotropy with an effective ferromagnetic exchange, show exotic short-range orders with macroscopic entropy[3] and peculiar excitations, where the R dipolar moments fractionalize into magnetic monopoles.[4] The spin liquid $Tb_2Ti_2O_7$ with weaker uniaxial anisotropy does not order either at long scale.[5] Here we focus on $Er_2Ti_2O_7$ with reversed behavior, namely, planar XY anisotropy and antiferromagnetic (AF) interactions, showing magnetic order below 1.2 K.[6]

$Er_2Ti_2O_7$ was proposed to realize a model type XY antiferromagnet, for which theory predicts a fluctuation-induced symmetry breaking, leading to magnetic long-range ordering.[7] Indeed, the crystal-field ground Kramers doublet of the Er^{3+} ion has an anisotropic g tensor:[8] $g_{\parallel}$=2.6 and $g_{\perp}$=6.8. Hence, the threefold symmetry [111] axis is a hard magnetic axis, the easy plane being the local (111) plane. Below T_N=1.2 K, the antiferromagnetic structure has a $\mathbf{k}$=0 propagation vector and it is defined by the basis vectors ψ_2, which transform according to the irreducible representation Γ_5, following the Kovalev notations. It corresponds to magnetic moments along ⟨211⟩ axes, as described in the drawings of Refs. 7 and 9.

The magnetic structure consists of six equally populated domains, as shown by spherical neutron polarimetry.[9] The selection of this particular state among the possible basis states of the $\mathbf{k}$=0 manifold is still subject to discussion. Surprisingly, it is the only noncoplanar structure among all others, whereas order by disorder processes usually select coplanar or collinear orders.[10] It also differs from the so-called Palmer-Chalker state,[11] predicted to be the ground state in the presence of AF isotropic exchange and dipolar interactions. An energetic selection of the ordered states was recently proposed,[12] arising from sixth-order terms in the crystal-field Hamiltonian, together with possible anisotropic exchange, dipolar and Dzyaloshinskii interactions. An anisotropic molecular field tensor with antiferromagnetic components, reinforcing the crystal-field planar anisotropy, has indeed been shown to be present in $Er_2Ti_2O_7$ using polarized neutron diffraction, by measuring the local susceptibility in the paramagnetic phase.[8]

The magnetic structure near T=0 has been shown to coexist with spin fluctuations by μSR spectroscopy:[13] a nonvanishing spin dynamics washes out the precession signal usually observed by muons in ordered magnets. This is confirmed by the presence of soft collective excitations probed by inelastic neutron scattering.[14] In this latter work, it

is shown that application of a magnetic field (along [110]) decreases the Néel temperature, resulting in a zero-temperature phase transition at a critical field $H_c \simeq 1.8$ T. The magnetic ordered state is suggested to transform into some kind of spin-liquid state above the critical field, through a second-order quantum phase transition driven by spin fluctuations.[12,14] The field evolution of the magnetic structure was qualitatively understood as a smooth deformation from the zero-field ψ_2 configuration to a field configuration above H_c, where the moments are aligned with or close to the field direction. In these studies, however, the spin configurations could not be characterized in detail, considering the limited information provided by the cold neutron measurements.

In this work, we present detailed in-field neutron-diffraction experiments in the AF phase of $Er_2Ti_2O_7$ using hot neutrons. This allows us to follow the evolution of the ground state induced by a magnetic field applied along [110], through the critical point and up to a field of 6 T, and to clarify both questions of the domain structure and of the microscopic local spin structure within a tetrahedron. We show that the Er moment magnitude presents a minimum around H_c, which can be considered as the spin-flip field for the [110] direction. Up to 6 T, the Er moments do not recover a fully collinear structure because [110] is not a principal direction for the local g tensor of half the Er sites. We apply a self-consistent calculation, in the molecular field approximation, to try and explain this evolution quantitatively; our model takes into account the crystal field interaction previously studied in Refs. 7 and 8, together with an anisotropic molecular field tensor, arising from exchange couplings with the six nearest neighbors of a given ion. We show that we can account for the field evolution of the magnetic structure in the AF phase (except in a limited field range below H_c) by the same molecular field tensor which accounts for the thermal variation in the local susceptibility in the paramagnetic phase.[8] We also apply our model to compute the lowest excitation energies at 0.05 K, the heat capacity in the paramagnetic phase, and the (H, T_N) phase diagram; a reasonable agreement is obtained with the experimental data of Refs. 7 and 14.

II. EXPERIMENTAL

A single crystal of $Er_2Ti_2O_7$ was grown by the floating-zone technique, using a mirror furnace, as described in Ref. 15. It was placed at the bottom of a dilution inset, inside a superconducting coil. The vertical axis of the magnetic field was aligned with the [110] axis, with a slight misorientation discussed below. Neutron-diffraction measurements were performed at the ORPHÉE reactor of the Laboratoire Léon Brillouin, on the Super-6T2 spectrometer in the unpolarized neutron version, with an incident neutron wavelength $\lambda_n = 0.9$ Å. The nuclear structure was characterized by zero-field neutron diffraction at two temperatures above T_N, 100 and 5 K, allowing the lattice constant, positional parameters, occupancy factors, isotropic temperature factors and extinction parameters to be refined, within the space group $Fd\bar{3}m$. To determine the magnetic structures, about 300 Bragg peaks were collected at 0.3 K, in zero field and for ten field values in the range 0–6 T.

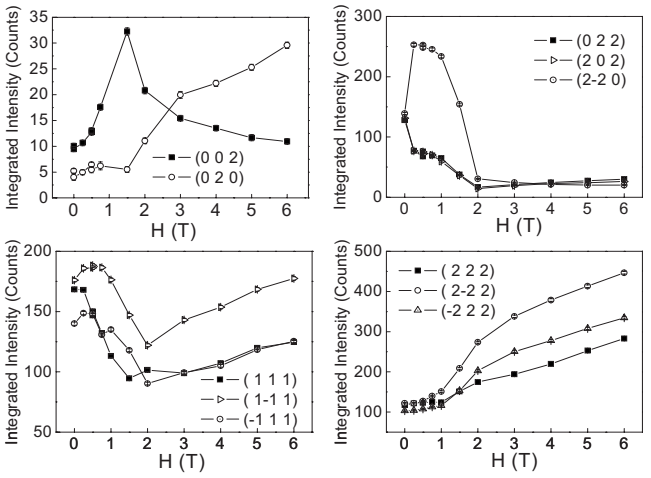

FIG. 1. Integrated intensities versus the field H applied along [110] of some typical Bragg peaks measured at 0.3 K in $Er_2Ti_2O_7$.

III. EVOLUTION OF THE MAGNETIC STRUCTURE

Figure 1 shows the field dependence of the integrated intensities of some particular Bragg peaks. The $(h,-h,l)$ peaks, situated in the horizontal plane, have a field dependence similar to that previously measured.[14] The lifting counter geometry of the diffractometer allowed us to measure the equivalent out-of-plane reflections plotted in the figure, which show different field dependencies. These allow several regions of interest to be distinguished. The low field region $H < 0.1$ T shows opposite variations of the $(2\bar{2}0)$ and (022)/(202) Bragg peaks, which are clearly assigned to the reorientation of the magnetic domains by the applied field. At higher fields, a single domain is stabilized and the variations in the Bragg peaks arise from moment reorientations inside a tetrahedron. The (002) and (111) Bragg peaks show an extremum at 1.5 T, somehow below the critical field. The evolution of the magnetic peaks with the field is well accounted for by the magnetic refinements described below.

Magnetic refinements were performed with the program FULLPROF.[16] In zero field, the magnetic structure is a $\mathbf{k}=0$ structure, which means that the four tetrahedra in the cubic unit cell have the same moment orientations. These orientations are those corresponding to the ψ_2 state, with moments in the easy planes along $\langle 211 \rangle$ axes. The magnetic moment at 0.3 K was refined as $m = 3.25(20)$ μ_B per Er ion. This value is much smaller than the free ion value $g_J J = 9$ μ_B, where $J = 15/2$ and the Landé factor $g_J = 6/5$ for Er^{3+}. The reduction is due to the crystal field, as described in Ref. 8 and below. The domain populations were refined, yielding three equally populated magnetic domains (together with the opposite domains giving the same contribution), as also found by polarized neutron measurements.[9]

Above 0.1 T, good refinements (with typical agreement factors $R_F = 5\%$) were obtained by considering a single magnetic domain. The evolution of the magnetic structure with

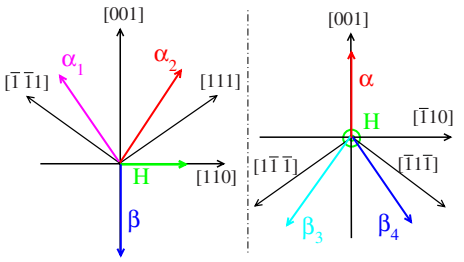

FIG. 2. (Color online) Zero-field configuration in the ψ_2 state in the $(\bar{1}10)$ (left) and (110) (right) plane. The [110] incipient field direction is indicated by a green arrow. The local trigonal axis (hard magnetic axis) for the α_1 (respectively, α_2) moments is [111] (respectively, $[\bar{1}\bar{1}1]$); for the β_3 (respectively, β_4) moments, it is $[\bar{1}1\bar{1}]$ (respectively, $[1\bar{1}\bar{1}]$). This configuration corresponds to that of the single domain occurring above 0.1 T. The upper (respectively, lower) hemisphere referred to in the text is that containing the positive (respectively, negative) part of the [001] axis.

the field was determined by refining the integrated magnetic intensities with moment values and angles as parameters. For the [110] field direction, the Er sites split into two sets, or chains: the α sites, with a local trigonal axis at an angle $\theta = \arcsin(1/\sqrt{3}) \simeq 35.3°$ from **H**, and the β sites with their local trigonal axis perpendicular to the field. In the ψ_2 state, the α sites split further into α_1 and α_2, with moments which are not symmetrical with respect to the field direction. We also split here the β moments into β_3 and β_4 (see Fig. 2). In our experimental setup, there is a slight misorientation of the applied field with respect to the [110] direction: the polar angle θ of the field is 93.8° (instead of 90°) and its azimuthal angle φ is 45.8° (instead of 45°). In the calculation described in the following section, we will neglect the small azimuthal misorientation and assume φ=45° but we take into account the exact θ value. In the refinements, in order to reduce the number of fitting parameters, we assumed equal magnitudes for the two β moments, which was *a posteriori* justified by the calculation. The preferred domain orientation (above a field of about 0.1 T) is such that the α moments lie in the upper hemisphere.

The moment orientations in a given tetrahedron are sketched for selected fields in Fig. 3. All the moments are seen to rotate toward the field direction (see c or d in Fig. 4) up to a field of about 2 T, which can be identified with the critical field H_c of Ref. 14. For this field value, all the moments are practically aligned along the field so that H_c can be considered as the spin-flip field of the $Er_2Ti_2O_7$ magnetic structure for the [110] field direction. On further increase in H beyond 2 T, the β moments remain along the field whereas the α moments tend toward an asymptotic orientation, symmetric with respect to **H**.

The data points in Fig. 4 represent the evolution of the moment values and orientations at the four Er sites as the field increases. Pronounced anomalies are seen in the critical region. As a major effect, all moment values show a minimum at H_c=2 T [Fig. 4(a)]. This minimum is much more pronounced for the α moments, which get the closest to their hard local trigonal axis for this field value. The α_1 moment decreases down to 1 μ_B whereas the α_2 moment reaches

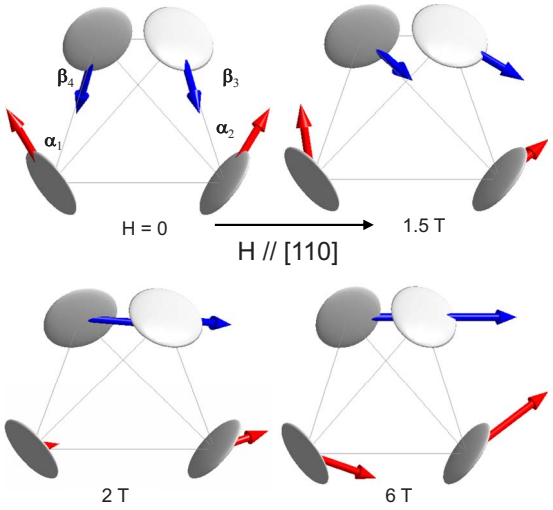

FIG. 3. (Color online) Evolution of the spin structure inside a tetrahedron for selected fields. The flat disks visualize the easy (111) planes. The α moments at the bottom of a tetrahedron are shown by red arrows and the β moments at the top by blue arrows with lengths proportional to the moment values.

2 μ_B. As to the β moments, which remain in their easy plane while rotating, they show a much shallower minimum of about 3 μ_B.

The evolution of the angles of the moments with the field is shown in Figs. 4(c) and 4(d). At 2 T, all the angles are close to zero. The "flip" of the α_1 moment is reflected by the change of sign of its angle with **H**, when it enters the lower hemisphere (see Fig. 2) above 2 T. By contrast, the α_2 moment approaches the field direction at 2 T, then tilts away, always remaining in the upper hemisphere. Above 2 T, the two α moments tend toward an orientation at 20°–25° on either side of the field. The β moments show a much smoother field variation: they progressively reorient toward the field and remain aligned along **H** from 2 T upward. The angles of the moments with their local trigonal axis [referred to as OZ in Fig. 4(b)] confirm that the β moments always remain in their easy plane while the α moments approach their hard axis in the critical region. Our model calculation, to be described in the next section, accounts for most features of this evolution.

IV. MODEL CALCULATION

We implemented a model intended to reproduce the experimental data concerning both the thermal variation in the local magnetic susceptibility in the paramagnetic phase, measured in Ref. 8, and the evolution with field of the magnetic structure at 0.3 K, measured in the present work. This model performs mean-field self-consistent calculations and uses as ingredients the crystal field parameters of Er^{3+} in $Er_2Ti_2O_7$ as in Ref. 8, and anisotropic two-ion exchange of the type

$$\mathcal{H}_{ex} = -\mathcal{J}_{\parallel} S_{1Z} S_{2Z} - \mathcal{J}_{\perp}(S_{1X} S_{2X} + S_{1Y} S_{2Y}), \qquad (1)$$

where $\mathcal{J}_{\parallel}$ and $\mathcal{J}_{\perp}$ are the components of the exchange tensor in the local frame with axial symmetry. We shall also con-

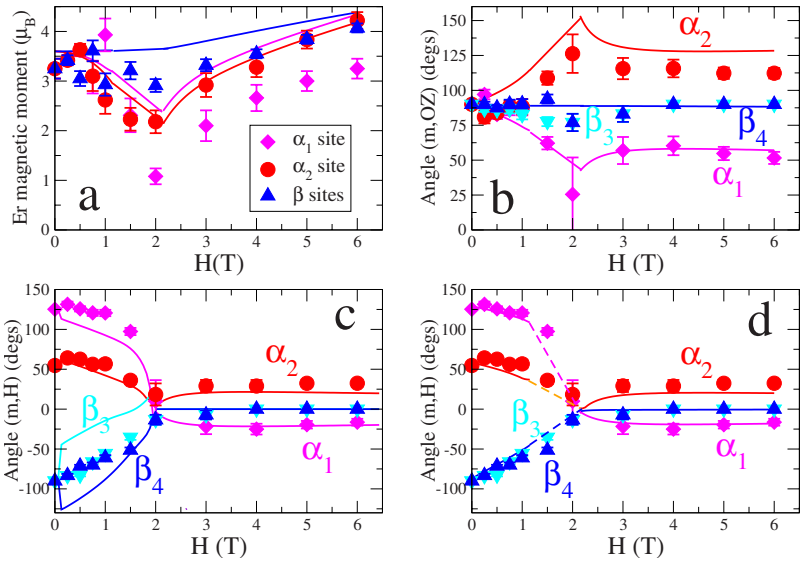

FIG. 4. (Color online) Variation with the field, applied along [110], of the moment magnitude (a) and orientation with respect to the local trigonal axis (b) and to the field direction (c and d), for the 4 Er sites in $Er_2Ti_2O_7$ at 0.3 K. Our convention for the angle with the field direction is that it is negative if the moment lies in the lower hemisphere. Solid lines in (a)–(c) are self-consistent calculations with $\lambda_\perp = -0.51\ \mathrm{T}/\mu_B$ and $\lambda_\parallel = -0.06\ \mathrm{T}/\mu_B$; solid lines in (d) are calculations with $\lambda_X = -0.54\ \mathrm{T}/\mu_B$, $\lambda_Y = -0.48\ \mathrm{T}/\mu_B$, and $\lambda_\parallel = -0.06\ \mathrm{T}/\mu_B$; dashed lines are interpolated ones.

sider the effect of a slight exchange anisotropy within the easy plane. We consider each ion in a tetrahedron to be exchange-coupled to its six nearest neighbors, resulting in an anisotropic molecular field tensor $\tilde{\lambda}$ such that the molecular field acting on this ion writes

$$\mathbf{H}_{\mathrm{mol}} = \frac{1}{6}\tilde{\lambda}\sum_{k=1}^{6}\mathbf{m}_k, \tag{2}$$

where the sum runs over the stx nearest neighbors. The relationship between the components of the $\tilde{\lambda}$ and $\tilde{\mathcal{J}}$ tensors is

$$\lambda_i = 6\mathcal{J}_i\left(\frac{g_J - 1}{g_J}\right)^2 \frac{1}{\mu_B^2}. \tag{3}$$

A self-consistent treatment involving the four Er moments, each with its three components, is performed, the only parameters being thus the two components $\lambda_\parallel$ and $\lambda_\perp$ of the $\tilde{\lambda}$ tensor in the local frame of axial symmetry. The dipolar coupling is not included in the calculation.

We apply first this model to the paramagnetic susceptibility and to the zero-field AF phase. In the paramagnetic phase, the $\chi_\parallel(T)$ and $\chi_\perp(T)$ data measured in Ref. 8 are very well reproduced using the above model with the axially symmetric AF molecular field tensor: $\lambda_\parallel = -0.06(3)\ \mathrm{T}/\mu_B$ and $\lambda_\perp = -0.51(4)\ \mathrm{T}/\mu_B$ (see Fig. 5). These values are close to those obtained in Ref. 8 using a simpler single sublattice model ($\lambda_\parallel = -0.15$, $\lambda_\perp = -0.45\ \mathrm{T}/\mu_B$). The planar anisotropy of the $\tilde{\lambda}$ tensor is strong ($\lambda_\perp/\lambda_\parallel \simeq 10$) and reinforces that of the crystal field. In the AF phase in zero field, the four Er moments in the ψ_2 ground state comply with the rule: $\Sigma_j \mathbf{m}_j = 0$, whence, for instance, $\mathbf{m}_2 + \mathbf{m}_3 + \mathbf{m}_4 = -\mathbf{m}_1$. Therefore, the molecular field acting on ion i is, according to Eq. (2): $\mathbf{H}^i_{\mathrm{mol}} = -\frac{1}{3}\lambda_\perp \mathbf{m}_i$, since the spontaneous moments lie in the easy plane. According to mean field theory, the transition temperature is given by: $k_B T_N = m_0 H_{\mathrm{mol}}$, hence in the ψ_2 state of $Er_2Ti_2O_7$: $k_B T_N = \frac{1}{3}|\lambda_\perp| m_0^2$, where the saturated moment m_0 and $\lambda_\perp$ must be obtained self-consistently in zero applied field and near 0 K. In order to obtain a transition temperature of 1.2 K, one needs the value $\lambda_\perp = -0.435\ \mathrm{T}/\mu_B$, which is remarkably close to that derived in the paramagnetic phase. This coherence gives confidence in the applicability of the molecular field approximation in the paramagnetic and AF phases of $Er_2Ti_2O_7$. The associated transverse exchange integral is $\mathcal{J}_\perp = -1.75$ K and the $T=0$ molecular field $H_{\mathrm{mol}} = 0.5$ T. The zero-field spontaneous moment is $m_0 = 3.52\ \mu_B$, close to the experimental value 3.25(20) μ_B, but somewhat higher than 3.00(05) μ_B measured in Ref. 7.

We then used the self-consistent exchange and crystal field model described above to calculate the evolution of the magnetic structure with increasing field. In a first step, we chose the two components of the axially symmetric $\tilde{\lambda}$ tensor as determined from the fit of the paramagnetic susceptibility ($\lambda_\perp = -0.51\ \mathrm{T}/\mu_B$ and $\lambda_\parallel = -0.06\ \mathrm{T}/\mu_B$). The results are displayed in Figs. 4(a)–4(c) as solid lines. The calculation does not exactly match the data but it captures the main trends of the rotation of the Er moments as the field is increased. Remarkably again, using the $\tilde{\lambda}$ tensor derived in the paramagnetic phase, the value of the critical or "spin-flip" field $H_c \simeq 2$ T is correctly reproduced. This value strongly depends

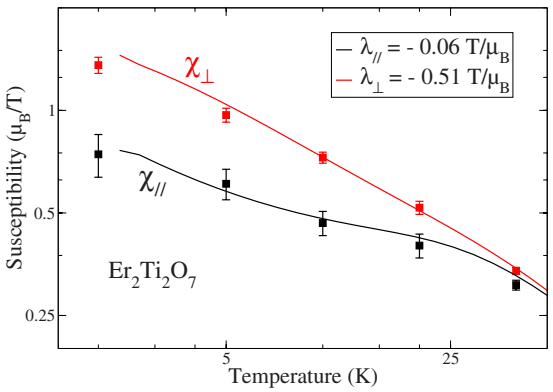

FIG. 5. (Color online) Low-temperature region of the thermal variation in the longitudinal and transverse susceptibilities in $Er_2Ti_2O_7$. The data are taken from Ref. 8 and the lines are calculated using the self-consistent model described in the text.

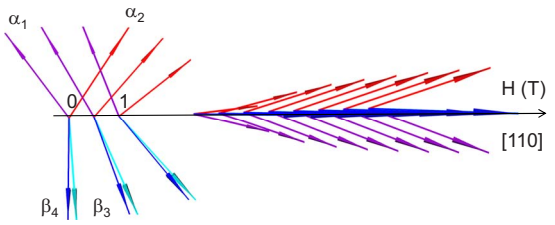

FIG. 6. (Color online) Evolution of the Er magnetic moments with the magnetic field at 0.3K, as calculated from the self-consistent calculation with $\lambda_X=-0.54$ T/μ_B, $\lambda_Y=-0.48$ T/μ_B, and $\lambda_\parallel=-0.06$ T/μ_B. Arrows are proportional to the moment values. Each field step corresponds to 0.48 T.

on $\lambda_\perp$ and very little on $\lambda_\parallel$. For a simple AF structure with moments perpendicular to the field, the spin-flip field in the presence of anisotropic $\tilde{g}$ and $\tilde{\lambda}$ tensors writes

$$H_{sf}=\frac{1}{2}g_\parallel\mu_B\left|\lambda_\parallel+\left(\frac{g_\perp}{g_\parallel}\right)^2\lambda_\perp\right|. \quad (4)$$

Since its moment configuration is more complicated than a two-sublattice AF structure, this expression cannot be directly applied to $Er_2Ti_2O_7$, but it accounts for the strong dependence of H_{sf} on $\lambda_\perp$ since $g_\perp/g_\parallel>1$ in $Er_2Ti_2O_7$.

However, as seen in Fig. 4(c), there is a discrepancy concerning the rotation of the β moments: the calculation yields different variations of the angle with the field for the two sites, whereas the data present identical variations within experimental uncertainties. This is due to a moment reorientation occurring in the calculation at a very small field (about 0.03 T): the moments jump from the ψ_2 state, with moments along the local OX axis of the $\langle 211\rangle$ family, to a configuration where each moment lies at about 38° from OX, which probably corresponds to the (small) potential well created by the crystal-field interaction. Since this reorientation is not observed in the data, one has to devise a mechanism which would reinforce the potential well along the local OX axis, at least at low field. For this purpose, in a second step, we lifted the in-plane degeneracy of the molecular field tensor by about 5%, through the introduction a slightly higher (absolute) value for λ_X than for λ_Y. The result of the calculation, with $\lambda_X=-0.54$ T/μ_B and $\lambda_Y=-0.48$ T/μ_B, is shown for the angle $\theta_H=(\mathbf{m},\mathbf{H})$ in Fig. 4(d) (the other calculated quantities remaining practically unchanged). The agreement is better for the β moments, i.e., the ψ_2 configuration evolves smoothly with increasing field, up to a field of 1.2 T. For $1.2<H<2$ T, the calculation presents an anomalous moment jump, still unexplained. Therefore, in Fig. 4(d), we do not consider the calculated curves in this field interval and we have drawn dashed lines interpolated between the lower and higher field regions where the model reproduces the data reasonably well. In Fig. 6, we show the evolutions of the four moments versus the magnetic field, calculated within this last model.

Finally, the high-field configuration is the following: the β moments lie along the field and the α_1 and α_2 moments are on either side of the field, at an angle of about 20°. This can

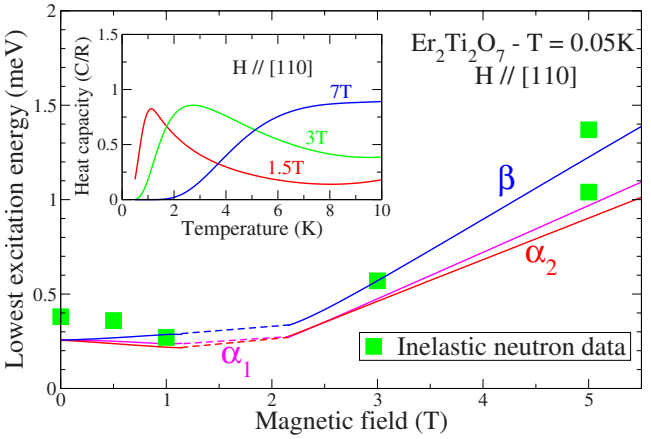

FIG. 7. (Color online) Calculated lowest excitation single ion energies for the four sites in $Er_2Ti_2O_7$, in the AF ordered phase at 0.05 K as a function of the applied magnetic field. The square dots are the (estimated) experimental values from Ref. 14, for fields where a clearly nondispersive level is observed in the inelastic neutron spectra. Insert: calculated thermal variation of the heat capacity for $H=1.5$, 3, and 7 T, obtained from the single-ion energies.

be understood since the [110] direction lies within the easy plane for the β moments whereas it is not a principal axis for the α moments.[17]

It is worth emphasizing here that the data cannot be reproduced with an *isotropic* molecular field constant $\lambda=-0.51$ T/μ_B. In this case, the calculation yields moments which remain in their easy plane up to the critical field of 2 T and this field is not a spin-flip field since the α moments do not align along its direction. The α moment magnitude then shows no minimum at 2 T. Therefore, our calculation, within its limits of validity, demonstrates the existence of an anisotropic molecular field tensor in $Er_2Ti_2O_7$.

The molecular field range is typically 0.5–1 T, which is much larger than the estimated magnitude of the dipolar field: $H_{dip}\simeq 5$ mT. This justifies the neglection of the latter in our calculation.

The influence of the slight misorientation of the applied field with respect to [110] is expected to be small because of the relative isotropy of the Er^{3+} g tensor and its planar character. In our calculation, it is reflected in the small degeneracy lifting of the $\alpha_1-\alpha_2$ branches in Fig. 4(a) (moment magnitudes) and in Fig. 7 (excitation energies). The field misorientation has a much more drastic effect[18,19] in the Ising-type systems $Ho_2Ti_2O_7$ and $Tb_2Ti_2O_7$.

V. DISCUSSION

In this section, we show that the model described above also accounts relatively well for other experimental results related to the spin excitations in $Er_2Ti_2O_7$, as previously measured by inelastic neutron scattering and heat capacity. In Refs. 7 and 14, a dispersionless mode was observed at about 0.4 meV for $H=0$, which further splits into higher energy modes when the field increases above the critical field. In first approximation, mostly valid in the middle of the Brillouin zone, such flat modes may be attributed to the splitting

of the ground Kramers doublet under the coupled influence of the external and exchange fields. In this picture, the splitting into several modes induced by the field can be understood by the different molecular fields experienced by the α and β moments. In Fig. 7, the excitation energies obtained by our model are compared with the energies of the flat modes determined in Ref. 14 (square dots in Fig. 7). Below 2 T, the calculated energies are almost field independent around 0.25 meV, and above this threshold field, they increase linearly with slightly different slopes. The data match reasonably well the calculated values, except at zero and low field, where the energy of the nondispersive mode (0.4 meV) is significantly above the calculation. One expects that our single ion mean-field energy calculation holds at high field, where exchange is small with respect to the Zeeman energy, but fails at low field. Indeed, at low field, one should consider, for instance, the system of four exchange coupled Er moments on a tetrahedron and calculate the whole spin-wave spectrum, taking altogether crystal field, exchange and Zeeman interactions into account.

In Ref. 14, the variation with field of the heat capacity in $Er_2Ti_2O_7$ was attributed to a crossover toward a quantum high field paramagnetic state reminiscent of that observed in the quantum critical magnet[20] $LiHoF_4$. We calculated the in-field heat capacity $C_p(T)$ in $Er_2Ti_2O_7$ below 10 K, using the crystal field and Zeeman energies of all the levels (see insert in Fig. 7). Whereas this simple Schottky-type calculation cannot capture the anomaly at the phase transition for low fields, it reproduces correctly the main features of the high field heat capacity data of Ref. 14. Especially, the smearing of the temperature dependence of $C_p(T)$ with increasing field can be correctly reproduced in this simple approach, which does not involves quantum fluctuations explicitly, besides the crystal-field interaction.

Finally, we also applied our model to the calculation of the ordering temperature as a function of the applied field, i.e., to the (H,T_N) phase diagram. With the $\tilde{\lambda}$ tensor determined above ($\lambda_x=-0.54$, $\lambda_y=-0.48$, and $\lambda_{\|}=-0.06$ T/μ_B), we calculated the thermal variation in the Er moments for different field values in the temperature range 0.2–2 K, in the field range below 1.3 T, where the model yields good agreement with experiment. As can be seen in Fig. 8, which displays the thermal variation of the α_1 moment magnitude, the ordering temperature, defined as the temperature where the moment variation shows a jump, decreases with increasing field.[21] This reflects the competition between the Zeeman and exchange energies, which leads to the critical point when the Zeeman coupling overwhelms exchange and prevents a spontaneous moment configuration to set in. The low field part of the (H,T_N) phase diagram is shown in the insert of Fig. 8. Our calculation is in qualitative agreement with the diagram obtained from the heat capacity data of Ref. 14. The curve $H=f(T_N)$ is seen to follow a power law (see dashed line in the inset of Fig. 8) with an exponent $n=2$. Extrapolation of this law to zero yields a critical field $H_c=f(T_N=0)=1.85$ T, close to the experimental value.

The above results shed some light on the nature of the critical point and high-field phase. Although a zero-temperature field-induced transition occurs at a critical field

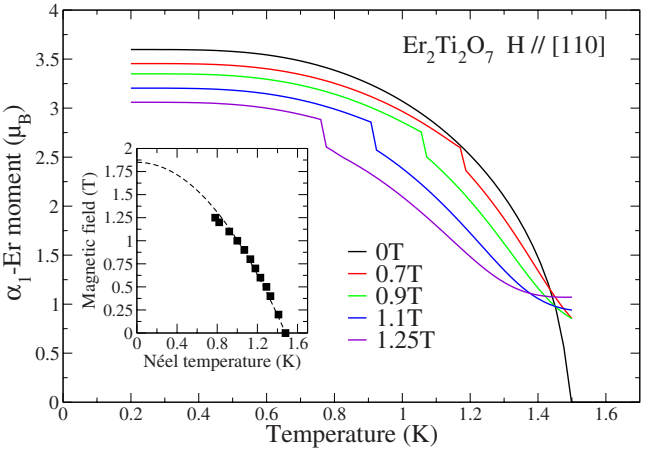

FIG. 8. (Color online) Calculated thermal variation in the α_1 Er moment in the presence of a magnetic field applied along [110], for different field values below 1.3 T, upper limit of validity of our model in the AF phase. Insert: (H,T_N) phase diagram obtained from the break-points of the α_1-site $m(T)$ curves. The dashed line represents the law $H=H_c[1-(\frac{T_N}{T_N^0})^2]$ with $H_c=1.85$ T and $T_N^0=1.48$ K.

$H_c \simeq 2$ T, it does not show obvious characteristics of a quantum phase transition. The field-induced transition can be well explained in a classical way by a competition between Zeeman and exchange energies. The geometrical frustration does not seem to play a major role in this behavior. The high-field state corresponds rather to a long-range ordered structure, with large magnetic moments and well defined spin waves, than to a quantum paramagnet. There is no obvious field-induced merging of the magnetic ground states at the critical point, as long as the main symmetry degeneracy (the classical domain structure) is relieved by a much lower field below 0.1 T. There is no level crossing at the critical point either, since the degeneracy of the ground state crystal field level is already lifted by the Zeeman-exchange energy (0.25 meV at H_c), which remains well below the lowest excitation energy of the crystal field (7 meV). This feature is at variance from quantum field induced phase transitions as observed in $LiHoF_4$ and molecular magnets.[20,22,23]

At the same time, one observes quite original features at the critical point, such as a collinear alignment of all magnetic moments along the field, which coincides with a minimum of the moment values, stronger than found in the calculation. These features could be accompanied by a softening of the spin waves and an enhancement of the local spin fluctuations and quasielastic neutron scattering.[14] A hallmark of quantum-critical transitions is the peculiar influence of the dynamics on the $T=0$ static critical behavior. A quantitative analysis of the spin wave spectrum would help to conclude if the above transition can be fully explained in a semi classical way, using the anisotropic exchange tensor described above, or if a more specific quantum approach is needed.

VI. CONCLUSION

Using neutron diffraction in the AF phase of the planar pyrochlore $Er_2Ti_2O_7$ with a magnetic field applied along

[110], we performed a quantitative study of the field evolution of the magnetic structure throughout the critical point at $H_c \simeq 2$ T. For this critical-field value, the AF magnetic structure has "flipped," i.e., all the Er moments are aligned along the field and their magnitude reaches a minimum. The strong decrease of the moment magnitude at H_c reflects the spin-wave damping and enhanced quasielastic scattering previously observed in neutron experiments. A four sublattice self-consistent calculation, taking into account exchange, Zeeman and crystal electric field interactions, accounts for most of the characteristics of the field-induced magnetic structure and critical point, from zero field up to well above H_c. It also explains semiquantitatively the field dependence of the heat capacity, of the dispersionless inelastic mode and of the transition temperature. The comparison between model and experiment brings out the strongly anisotropic exchange interaction ($\mathcal{J}_\perp / \mathcal{J}_\parallel \simeq 10$) as a necessary ingredient to explain all the features of the critical point. The critical field can then be defined as the field value for which the Zeeman energy overcomes the exchange energy, taking the anisotropic exchange tensor into account. The anisotropic exchange, already outlined by local susceptibility measurements in the paramagnetic phase, should also influence the spin-wave excitation spectrum in the AF ordered phase.

ACKNOWLEDGMENTS

We acknowledge very fruitful discussions with C. Lacroix (Institut Louis Néel, Grenoble) and J. Robert (LLB Saclay). Huibo Cao acknowledges supports from the Triangle de la Physique.

*isabelle.mirebeau@cea.fr

[1] J. Villain, R. Bidaux, J.-P. Carton, and et R. Conte, J. Phys. (Paris) **41**, 1263 (1980).
[2] J. T. Chalker, P. C. W. Holdsworth, and E. F. Shender, Phys. Rev. Lett. **68**, 855 (1992).
[3] S. T. Bramwell and M. J. P. Gingras, Science **294**, 1495 (2001).
[4] C. Castelnovo, R. Moessner, and S. L. Sondhi, Nature (London) **451**, 42 (2008).
[5] J. S. Gardner, S. R. Dunsiger, B. D. Gaulin, M. J. P. Gingras, J. E. Greedan, R. F. Kiefl, M. D. Lumsden, W. A. MacFarlane, N. P. Raju, J. E. Sonier, I. Swainson, and Z. Tun, Phys. Rev. Lett. **82**, 1012 (1999).
[6] H. W. J. Blöte, R. F. Wielinga, and W. J. Huiskamp, Physica **43**, 549 (1969).
[7] J. D. M. Champion, M. J. Harris, P. C. W. Holdsworth, A. S. Wills, G. Balakrishnan, S. T. Bramwell, E. Čižmár, T. Fennell, J. S. Gardner, J. Lago, D. F. McMorrow, M. Orendáč, A. Orendáčová, D. McK. Paul, R. I. Smith, M. T. F. Telling, and A. Wildes, Phys. Rev. B **68**, 020401(R) (2003).
[8] H. Cao, A. Gukasov, I. Mirebeau, P. Bonville, C. Decorse, and G. Dhalenne, Phys. Rev. Lett. **103**, 056402 (2009).
[9] A. Poole, A. S. Wills, and E. Lelièvre-Berna, J. Phys.: Condens. Matter **19**, 452201 (2007).
[10] J. T. Chalker, in *Introduction to Frustrated Magnetism*, edited by C. Lacroix, P. Mendels, and F. Milla (Springer, Berlin, in press).
[11] S. E. Palmer and J. T. Chalker, Phys. Rev. B **62**, 488 (2000).
[12] P. A. McClarty, S. H. Curnoe, and M. J. P. Gingras, J. Phys.: Conf. Ser. **145**, 012032 (2009).
[13] J. Lago, T. Lancaster, S. J. Blundell, S. T. Bramwell, F. L. Platt, M. Shirai, and C. Baines, J. Phys.: Condens. Matter **17**, 979 (2005).
[14] J. P. C. Ruff, J. P. Clancy, A. Bourque, M. A. White, M. Ramazanoglu, J. S. Gardner, Y. Qiu, J. R. D. Copley, M. B. Johnson, H. A. Dabkowska, and B. D. Gaulin, Phys. Rev. Lett. **101**, 147205 (2008).
[15] G. Balakrishnan, O. A. Petrenko, M. R. Lees, and D. McK. Paul, J. Phys.: Condens. Matter **10**, L723 (1998).
[16] J. Rodriguez-Carvajal, Physica B **192**, 55 (1993).
[17] Actually, for an isolated Kramers doublet, if the field is at an angle θ from the symmetry axis, then the angle γ of the magnetic moment with the axis is given by: $\tan \gamma = (\frac{g_\perp}{g_\parallel})^2 \tan \theta$. Inserting the zero-field g values in this expression leads to an asymptotic angle of the moment with respect to **H** of $\simeq 40°$, instead of the actual 20°. This discrepancy arises from the mixture of the excited crystal field states into the ground state by the Zeeman effect, which modifies the g values.
[18] A. Sazonov, A. Gukasov, I. Mirebeau, H. Cao, P. Bonville, B. Grenier, and G. Dhalenne, arXiv:1008.2979 (unpublished).
[19] J. P. Clancy, J. P. C. Ruff, S. R. Dunsiger, Y. Zhao, H. A. Dabkowska, J. S. Gardner, Y. Qiu, J. R. D. Copley, T. Jenkins, and B. D. Gaulin, Phys. Rev. B **79**, 014408 (2009).
[20] H. M. Rønnow, R. Parthasarathy, J. Jensen, G. Aeppli, T. F. Rosenbaum, and D. F. McMorrow, Science **308**, 389 (2005).
[21] With the mean value $\lambda_\perp = -0.51$ T/μ_B, the calculated T_N value in zero field is 1.48 K, rather than the experimental value 1.2 K. This probably reflects a small imperfection of the model, which requires a 15% higher $\lambda_\perp$ value to account for the in-field properties than for the zero-field T_N value.
[22] D. Bitko, T. F. Rosenbaum, and G. Aeppli, Phys. Rev. Lett. **77**, 940 (1996).
[23] Bo Wen, P. Subedi, Lin Bo, Y. Yeshurun, M. P. Sarachik, A. D. Kent, A. J. Millis, C. Lampropoulos, and G. Christou, Phys. Rev. B **82**, 014406 (2010).